A new perspective on increased emergence of Central Pacific ENSO in the recent two decades

Shangfeng Chen
Chinese Academy of Sciences
Wen Chen (cw@post.iap.ac.cn)
Institute of Atmospheric Physics, Chinese Academy of Sciences https://orcid.org/0000-0001-9327-9079
Bin Yu
Climate Research Division, Environment and Climate Change Canada
Renguang Wu
School of Earth Sciences, Zhejiang University https://orcid.org/0000-0003-4712-2251
Hans Graf
University of Cambridge
Lin Chen
Nanjing University of Information Science and Technology

Article

Keywords:

Posted Date: April 21st, 2022

DOI: https://doi.org/10.21203/rs.3.rs-1549156/v1

Abstract

In this study, we provide a new perspective on the recent increased emergence of the central Pacific type of El Niño and Southern Oscillation (ENSO). Our results indicate that early-spring Aleutian Low (AL) intensity has a remarkable impact on the following winter ENSO especially after the late-1990s. Decrease (increase) in the early-spring AL strength tends to induce an anomalous cyclone (anticyclone) over subtropical North Pacific via wave-mean flow interaction. The anomalous cyclone (anticyclone) leads to sea surface temperature (SST) increase (decrease) in the equatorial Pacific in the following summer via wind-evaporation-SST feedback and trade wind charging mechanism, which further contributes to succeeding central Pacific-like El Niño (La Niña). This remarkable AL's impact on ENSO is attributable to enhancement of the background trade winds, which is related to changes of both the AMO and NPGO from positive to negative phases around the late-1990s. In contrast, global warming is suggested to have a negative effect on the recent increased connection of the early-spring AL with the following winter ENSO. The results offer the potential to advance our understanding of the factors that explain decrease of the prediction skill of ENSO since the late-1990s.

1. Introduction

The El Niño and Southern Oscillation (ENSO) is the dominant mode of the tropical air-sea coupling system[1–4], featured by large sea surface temperature (SST) anomalies in the tropical central and eastern Pacific, and accompanied by notable changes in the tropical atmospheric circulation and convection. Although ENSO is a climate system in the tropical Pacific, it has tremendous impacts on the climate, agriculture, ecosystems, water resource and the livelihoods of people worldwide[5–10]. Therefore, identifying the factors leading to the occurrence of ENSO event and improving the prediction skill of ENSO are of critical importance.

The prediction skill of ENSO is found to decrease obviously since the late-1990s[11–12], corresponding to the time when the central Pacific (CP) type of El Niño has occurred more frequently[13–15]. Extratropical atmospheric forcings over the North Pacific, particularly the North Pacific Oscillation (NPO, the second Empirical Orthogonal Function [EOF] mode of sea level pressure anomalies [SLP] over the North Pacific[16]), are suggested to contribute significantly to the occurrence of the CP ENSO via the seasonal footprinting mechanism and trade wind charging mechanism[17–23]. However, recent studies indicated that the impact of the winter NPO on the following winter ENSO weakens largely after the late-1990s[24–25], suggesting that winter NPO cannot well explain the recent increased emergence of the CP ENSO.

Then, what might be the main factor that caused the frequent occurrence of CP ENSO events after the late-1990s? This study finds that the early-spring (March) Aleutian Low (AL) plays an important effect, although prevailing view generally suggested a marked impact of the ENSO on the AL rather than the opposite effect[6,26–27]. The AL represents the first leading mode of atmospheric variability over the North Pacific and explains more variance than the NPO[18] (Supplementary Fig. 1). A recent study has

preliminarily recognized that variation in the early-spring AL intensity has a marked impact on the following winter ENSO[28]. However, whether the recent increased occurrence of CP ENSO is related to the impact of the early-spring AL remains unclear. In this study, we demonstrate that the significant impact of the early-spring AL on the following winter ENSO occurred only after the late-1990s. We suggest that the early-spring AL may play a more important role than the winter NPO in the increased occurrence of the CP type ENSO events during recent decades. The role of the interdecadal climate variability and global warming to the recent enhanced connection of the early-spring AL with the following winter ENSO are also discussed.

3. Strengthened Impact Of The March Al On Enso

The connection of the March AL with the following winter ENSO shows a stepwise increase over period of 1948–2020 (Fig. 1a). The significant relationship of the March AL index (ALI, Methods) with the following winter Niño-3.4 SST index can only be observed after the late-1990s (Fig. 1a), in line with the time that CP type ENSO events became more frequent[13–15,18–20]. After the late-1990s, 7 out of 8 weakened AL years (Methods) are followed by El Niño events in the subsequent winter (supplementary Table 1). The occurrences of the recent five CP El Niño events (i.e., 2002-03, 2004-05, 2006-07, 2009-10 and 2015-16) are all preceded by weakened AL years. In addition, 6 out of the 7 enhanced AL years are followed by La Niña events. This result suggests that the occurrence ratio of ENSO events is near 90% associated with the March AL after the late-1990s. Thus, the impact of the March AL on the tropical Pacific SST is suggested to be an important factor for the increased occurrence of the CP-type ENSO events since the late-1990s.

Studies generally suggested that the recent increased occurrence of the CP ENSO events was related to the winter NPO-related atmospheric forcing[19–20]. The correlation of the winter NPO index (Methods) with the following winter Niño-3.4 SST index becomes weaker and insignificant after the late-1990s (Fig. 1b), consistent with recent studies[24–25]. Particularly, the correlation between the winter NPO index and following winter Niño-3.4 SST index is only 0.34 (cannot past the 90% confidence level) after the late-1990s, about half of the correlation between the March ALI and the following winter Niño-3.4 SST index ($r = 0.63$). In addition, after the late-1990s, only 3 of 6 (4 of 7) positive (negative) winter NPO years are followed by El Niño (La Niña) events (Supplementary Table 1). The occurrence ratio of ENSO events is about 50% under condition of the winter NPO after the late-1990s, much lower than that of March AL. Moreover, the three positive winter NPO years (i.e., 2005-06, 2010-11, and 2011-12) are even followed by La Niña events in the following winter. Above results suggest that the March AL plays a more important role for the increased occurrence of the CP ENSO events after the late-1990s compared to the NPO.

4. Mechanisms For The Strengthened Impact Of The Al On Enso

It is necessary to understand the causes for appearance of the recent significant impact of the March AL on the following winter ENSO. According to Fig. 1a, we separate the entire period into two sub-periods:

1949–1995 and 1996–2020. The difference in the correlation coefficient between periods 1996–2020 (r = 0.63) and 1949–1995 (r = 0.12) is significant at the 99% confidence level according to the Fisher's r-z transformation (Methods).

After the late-1990s, the weakened AL in preceding March is associated with a dipole atmospheric anomaly pattern over the North Pacific (Fig. 2a). Formation of the anomalous cyclone over the subtropical North Pacific is attributable to the interaction between mean flow and synoptic-scale eddy activity[28]. The subtropical cyclonic anomaly reduces the total wind speed and leads to ocean surface warming over subtropical northeastern Pacific in the late-spring via reduction of surface heat flux (Fig. 2g). SST anomaly pattern in Fig. 2g bears a resemblance to the Pacific meridional mode (PMM)[29–30]. The late-spring ocean surface warming in the subtropical North Pacific extends southward to the equatorial central Pacific via wind-evaporation-SST feedback mechanism[29,31–32], which further develop to an El Niño event in the following winter via Bjerknes-like positive air-sea interaction[1] (Figs. 2b-e and 2g-j). The early-spring AL could also impact the following winter ENSO via the oceanic processes, mainly the trade wind charging mechanism[22–23]. Specifically, the cyclonic anomalies over the subtropical North Pacific induced by the AL reduce the trade winds and induce negative wind stress curl anomalies over the tropical central Pacific (Supplementary Fig. 2f), which leads to downward Ekman Pumping and meridional Sverdrup transport toward the tropical central Pacific. This results in increase in sea surface height and significant subsurface warming in the tropical central Pacific in the following summer (Supplementary Figs. 2c, 2h), which further impact the following winter ENSO occurrence[2–23,33–34].

Before the late-1990s, an atmospheric dipole anomaly pattern also appears over the North Pacific (Supplementary Fig. 3a). However, the subtropical anomalous cyclone is much weaker. Correspondingly, ocean surface warming is less obvious in the subtropical northeastern Pacific (Supplementary Fig. 3g) compared to that after the late-1990s (Fig. 2g). Therefore, March AL-related SST and atmospheric anomalies cannot extend to the tropical central Pacific, and thus have weak impacts on the following winter ENSO (Supplementary Figs. 3g-j).

Above analysis indicates that the most important system in connecting the March AL to the following winter ENSO is the cyclonic anomaly over the subtropical North Pacific, and associated westerly wind anomalies over the tropical western-central Pacific (TWCP). Figure 3a shows a scatter plot between the 23-yr moving correlations of the March AL with the following winter ENSO against the corresponding AL-related westerly wind anomalies over the TWCP in AM(0). It shows that in decades when the March AL-related westerly wind anomalies over the TWCP is strong (weak), impact of the March AL on the following winter ENSO is strong (weak) (Fig. 3a).

What are the plausible factors for the change of the March AL-related westerly wind anomalies over the TWCP? The amplitude of the March AL-related cyclonic anomaly over the subtropical western-central North Pacific after the late-1990s (Fig. 2a) is approximately two times stronger than that before the late-1990s (Supplementary Figs. 3a). The stronger cyclonic anomaly over the subtropical North Pacific can lead to stronger westerly wind anomalies to its south side over the TWCP. This can be clearly verified by a

scatter plot of the March AL-related westerly wind anomalies over the TWCP against the March AL-related SLP anomalies over the subtropical western-central North Pacific (Fig. 3b). In decades when the March AL-generated cyclonic anomaly over the subtropical western-central North Pacific is stronger, stronger westerly wind anomalies are induced over the TWCP (Fig. 3b). This further contributes to a stronger influence of the March AL on the following winter ENSO (Fig. 3c).

The interaction between the synoptic-scale eddy activity and low frequency mean flow plays an important role in the formation of the March AL-related cyclonic anomaly over the subtropical North Pacific[28]. A stronger cyclonic anomaly implies a stronger synoptic-scale eddy activity feedback to the mean flow. Strength of the synoptic-scale eddy activity feedback to mean flow is impacted by the zonal wind anomalies induced by the AL and the mean state of the background zonal wind over the mid-latitude North Pacific[35–39]. Stronger zonal wind anomalies can lead to strengthened feedback of the synoptic-scale eddy to low frequency flow if background mean flow is the same[37–39]. Similarly, if the amplitude of the zonal wind perturbation is the same, strength of the synoptic-scale eddy feedback to mean flow is closely associated with the intensity of the background zonal wind[37–39].

A scatter plot of the March AL-related SLP anomalies averaged over the subtropical western-central North Pacific against the AL-related SLP anomalies averaged over the mid-latitude North Pacific shows that the change in the strength of the March AL-related atmospheric anomaly over subtropical North Pacific is not due to change in the amplitude of the AL (Supplementary Fig. 4). It implies that the change in the background zonal wind should be a factor for the difference in the AL-related cyclonic anomaly over the subtropical North Pacific. To confirm this, we construct a scatter plot of the March AL-related SLP anomalies over the subtropical western-central North Pacific against the strength of the climatological 500-hPa zonal wind averaged over the mid-latitude North Pacific in Fig. 3d. Overall, when the mid-latitude background zonal wind is stronger, the easterly wind anomalies over the mid-latitude North Pacific lead to a stronger cyclonic anomaly over the subtropical North Pacific (Fig. 3d) via wave-mean flow interaction[28,35–39], which contributes to stronger westerly wind anomalies over the TWCP (Fig. 3b) and results in a marked impact of the March AL on the winter ENSO (Fig. 3c).

In addition, the air-sea interaction (i.e., the WES feedback) in the subtropical northeastern Pacific also plays a crucial role in maintaining and extending the March AL-related atmospheric and SST anomalies over the subtropics to the deep tropics, which further exert impacts on the occurrence of the following winter ENSO[29,40–41]. The weakened March AL-generated cyclonic anomaly before the late-1990s cannot induce SST warming in the subtropical northeastern Pacific (Supplementary Fig. 3g). This is in sharp contrast to the pronounced warming in the subtropical northeastern Pacific after the late-1990s (Fig. 2g). This implies that the air-sea interaction strength (i.e., WES feedback strength, Methods) should be much stronger after the late-1990s. The stronger WES feedback over the subtropical northeastern Pacific is favorable to the southwestward propagation of atmospheric variability from the extratropical North Pacific to the tropical central Pacific (Supplementary Fig. 5), and thus exerts impacts on ENSO[41–42]. Connections of the air-sea coupling strength over the subtropical northeastern Pacific with the March AL-

related low-level westerly wind anomalies over the TWCP (Fig. 3e) and with the running correlations between the March ALI and winter Niño3.4 SST index (Fig. 3f) clearly show that when the air-sea coupling is stronger over the subtropical northeastern Pacific, the March AL-generated westerly wind anomalies are stronger over the TWCP (Figs. 2g and 3e), which further contribute to a stronger impact of the AL on the winter ENSO (Fig. 3f).

Mean state of the circulation, especially the climatology of trade wind over subtropical northeastern Pacific, plays a dominant role in determining the strength of the WES feedback (Methods)[21,40,43]. Particularly, the strength of the WES feedback is determined by the ratio of the background wind perturbation and the mean zonal wind (Methods). The stronger mean zonal wind (i.e., easterly) leads to an enhanced upward latent heat flux for the similar wind speed anomalies, corresponding to a stronger air-sea coupling strength and the increased WES feedback efficiency. Therefore, the stronger the subtropical high and the northeasterly trade wind over the subtropical northeastern Pacific results in a larger air-sea coupling strength, which contributes to stronger March AL-related westerly wind anomalies over the TWCP, and thus leads to an increased impact on the following winter ENSO.

The background spring SLP over the subtropical northeastern Pacific (east of the Hawaiian Islands) is indeed significantly higher after than before the late-1990s, indicating a strengthened subtropical High there (Fig. 4a). Correspondingly, notable easterly wind differences are seen over the subtropical northeastern Pacific, indicating strengthened trade winds (Fig. 4b). The strengthened subtropical High and northeasterly trade winds increase the efficiency of the WES feedback, which contributes to stronger westerly wind anomalies over the TWCP in association with the March AL variation. This assertion can be further confirmed by scatter plots of the March AL-related spring 850-hPa zonal wind anomalies over the TWCP against climatological mean spring SLP and spring 850-hPa zonal wind over the subtropical northeastern Pacific in Fig. 4c and Fig. 4d, respectively. The correlation coefficients of the March AL-related westerly wind anomalies averaged over the TWCP with the spring climatological mean SLP and 850-hPa averaged over the subtropical Northeastern Pacific for the 23-yr running period are as high as 0.86 and 0.8. Hence, changes in the mean state of the subtropical high and northeasterly trade winds over the subtropical northeastern Pacific are suggested to play an important role in the formation of the TWCP westerly wind anomalies related to the spring AL, via modulating efficiency of the WES feedback. This further determines the strength of the impact of the March AL on the following winter ENSO. It is noted that the strengthened subtropical High around the late-1990s could have also contributed to the strengthened climatology westerly wind over the mid-latitude North Pacific, which leads to increased wave-mean flow interaction and results in stronger AL-related cyclonic anomaly over the subtropical North Pacific as discussed above.

5. Role Of The Internal Climate Variability And Anthropogenic Forcing

Above analysis indicates that the strengthened air-sea coupling over the subtropical northeastern Pacific due to the strengthened trade winds is crucial for the increased impact of the March AL on the following winter ENSO after the late-1990s. The late-1990s is also the time that the Atlantic Multidecadal

Oscillation (AMO) shifts from its negative to positive phase[44,45] (Fig. 5a). Spring SLP and easterly winds over the subtropical northeastern Pacific are significantly stronger during a positive AMO phase compared to a negative AMO phase (Figs. 5c and 5e). Thus, the AMO phase shift may lead to strengthened subtropical high and background trade winds over the subtropical Northeastern Pacific, which can result in increased efficiency of the WES feedback, favorable for strong impacts of the March AL on the winter ENSO after the late-1990s.

In addition to the AMO, Pacific Decadal Oscillation (PDO) and North Pacific Gyre Oscillation (NPGO) are also important interdecadal climate variability modes over the North Pacific. SLP and zonal wind anomalies over the subtropical northeastern Pacific are weak around 10^{o}-20^{o}N between positive and negative PDO phases (Supplementary Figs. 6b and 6c). This suggests that the phase change of the PDO does not likely contribute to the increased air-sea coupling after the late-1990s. By contrast, a positive NPGO phase contributes to stronger spring SLP and easterly winds over the subtropical northeastern Pacific (Figs. 5d and 5f). This implies that the change of the NPGO from its negative to positive phases around the late-1990s may also has a considerable contribution to the increased air-sea coupling and the strengthened spring AL-ENSO connection via enhancing the subtropical high and trade winds. In addition, the NPGO is in its negative phase before the early-1960s, which contributes to weakened subtropical high and trade winds over the subtropical northeastern Pacific. The possible interference of the negative NPGO phase may be a reason why the previous positive phase of the AMO (during 1930s-1960s) was not accompanied by enhanced spring AL-winter ENSO connection.

Besides the interdecadal climate variability, it is interesting to explore whether global warming has a contribution to the enhancement of the background northeasterly trade winds over the subtropical northeastern Pacific. To address this issue, we have calculated the differences in spring mean 850-hPa zonal wind between historical simulations over 1920–1999 and SSP-585 simulations over 2020–2099 from 34 CMIP6 models (Supplementary Fig. 7). All the individual CMIP6 models, as well as their ensemble mean, project weakened trade winds over the subtropical northeastern Pacific under the global warming (Supplementary Fig. 7). To exclude the possible impact of the internal climate variability, we have also used the 50-member large ensemble simulations conducted with the CanESM2. Differences in spring mean 850-hPa zonal wind over periods 2045–2100 (following RCP85 scenario) and 1950–2005 (historical simulation) in the 50 individual members and their ensemble mean confirm a weakened springtime trade wind over the subtropical northeastern Pacific under global warming (Supplementary Fig. 8). Overall, global warming leads to decrease in climatological mean springtime trade wind, which may suppress the air-sea coupling over the subtropical northeastern Pacific. Hence, global warming may have a negative contribution to the recent increased impact of the March AL on the following winter ENSO.

6. Conclusion And Discussion

This study reveals a pronounced impact of the March AL on the subsequent winter ENSO after the late-1990s, which may play a critical role for the increased occurrence of CP ENSO events during recent

decades. The change in the March AL-winter ENSO connection is found to be related to the change in the mean state of atmospheric circulation over the North Pacific. The strong mean zonal wind over the mid-latitude North Pacific after the late-1990s leads to increased wave-mean flow interaction, and results in strengthened cyclonic anomaly over the subtropical North Pacific and westerly wind anomalies over the TWCP. This contributes to a stronger impact of the March AL on the following winter ENSO. In addition, strong mean trade winds after the late-1990s lead to increased air-sea coupling and WES feedback over the subtropical northeastern Pacific. Thus, the March AL-generated cyclonic anomaly and ocean surface warming in the subtropics can easily penetrate to the deep tropics and impact the following winter ENSO. Our analysis also indicates that changes of both the AMO and NPGO from positive to negative phases around the late-1990s contribute to the enhancement of the mean trade wind and WES feedback over the subtropical northeastern Pacific. In contrast, global warming tends to decrease the mean state of the trade wind over the subtropical northeastern Pacific, and is thus suggested to have a negative effect on the recent increased connection of the early-spring AL with the following winter ENSO via suppressing the air-sea coupling.

Our study indicates that, after the late-1990s, a weaker (stronger) early-spring AL intensity tends to induce an El Niño (La Niña) event in the following winter. Previous studies demonstrated that an El Niño (a La Niña) event tends to lead to a strengthened (weakened) AL[6,26–27]. Hence, an El Niño event in the first year can be followed by a La Niña event in the second year with the feedback from the strengthened spring AL. Similarly, a La Niña in the first year can be followed by an El Niño event in the second year with a feedback from the weakened spring AL. This implies that the AL-ENSO interaction may serve as an important phase-transition mechanism during the ENSO cycle with a period of about 2 years, resulting in the quasi-biennial component of the ENSO. Previous studies have demonstrated that the CP type of ENSO shows a significant quasi-biennial component[45–46]. In addition, the quasi-biennial component of ENSO is suggested to be the major factor responsible for the spring persistence barrier of ENSO[46]. Therefore, considering the spring AL may to some extent help reduce the spring predictability barrier of ENSO in the current coupled climate models and improve the prediction of ENSO. However, in order to employ the spring AL to forecast ENSO events, the current state of the art coupled climate models should have to be able to realistically simulate the AL variation as well as the physical process linking the early-spring AL with the following winter ENSO. These issues will be explored in the near future.

Declarations

Declarations

Competing Interests:

The authors declare no competing interests

Authors contributions:

S.C. and W.C. conceived the study, performed the analyses and wrote the manuscript. B.Y., R.W., H.G. and L.C. contributed to revising the paper and assisted in interpretation of the results.

Acknowledgments:

This study was supported jointly by the National Natural Science Foundation of China (Grants 42175039, 41961144025 and 41721004), and the Jiangsu Collaborative Innovation Center for Climate Change.

Methods

Observations and reanalysis data

We use the monthly mean SLP, winds at 850-hPa and 500-hPa, and precipitation rate provided by the National Centers for Environmental Prediction-National Center for Atmospheric Research reanalysis dataset from January 1948 to the present[47], and monthly mean SST provided by the National Oceanic and Atmospheric Administration (NOAA) Extended Reconstructed SST version 5 from January 1854 to the present[48]. Monthly mean precipitation data from January 1979 to the present are obtained from the Climate Prediction Center Merged Analysis of Precipitation (CMAP) dataset[49]. In addition, monthly mean surface wind stress, sea surface height, and subsurface sea water potential temperature are extracted from the Global Ocean Assimilation System reanalysis dataset from January 1980 to the present[50]. Subsurface sea water potential temperature extends from 5 m to 4478 m below sea level.

Historical simulations of CMIP6

To examine the effect of global warming on the background circulation, we compare the historical simulations and the climate change projection simulations under the SSP585 scenario from 34 coupled climate models that participated in CMIP6[51] (Supplementary Table 2). As a number of models only provide one member in the historical simulation or the climate change simulation, we only employ the first run from these 34 CMIP6 models. Mean state differences of interested variables between SSP585 scenario (2020-2099) and historical (1920-1999) simulations from the 34 CMIP6 models are used to represent the influence of the global warming. Note that we use the 80-year mean to reduce the impact of internal climate variability.

Large ensemble simulations of CanESM2

We use the 50-member large ensemble climate simulations conducted with the second-generation Canadian Earth System Model to further confirm the effect of the global warming on the mean climate, which largely exclude the contribution of the internal climate variability (CanESM2)[52-53]. The 50-member

climate simulations of CanESM2 are briefly summarized as follows. First, five simulations are constructed over 1850-1950 to develop five different oceanic conditions in 1950. Second, ten simulations are further performed from each of the above five simulations with small different initial conditions in 1950. Due to the chaotic nature of climate systems, the small different initial condition in 1950 results in quite different atmospheric states a few days later[54]. This produces 50 members of simulations over the period 1950-2100. Over 1950-2005, each of the simulations is forced with the same historical radiative forcings, sulfate aerosols, and greenhouse gas concentration. Over 2006-2100, the simulations are forced by the RCP8.5 scenario forcing[55]. We compare the mean state differences between 2045-2100 and 1950-2005 in the CanESM2 simulations. Because each of the simulations is forced by the same external forcing with only slight differences in the initial condition, the difference of the projected changes among the 50 members is due solely to internal climate variability. In addition, projected changes due to the external forcing can be obtained by averaging the results of the CanEMS2 50 members.

PMM and air-sea coupling strength

Studies have indicated that the PMM is the first leading air-sea coupling mode over the subtropical Northeastern Pacific[29-30,41]. The PMM is defined as the first singular value decomposition (SVD, also called maximum covariance analysis, MCA) mode of the SST and surface winds anomalies over the subtropical Northeastern Pacific[29-30,41]. As in previous studies, strength of the air-sea coupling (i.e., WES feedback) over the subtropical northeastern Pacific is defined as the correlation coefficient between the PMM-SST and PMM-wind indices[41-42,56]. The PMM-SST (PMM-wind) index is represented by expansion coefficient time series of SST (surface winds) corresponding to the first SVD of SST and surface winds over the subtropical Northeastern Pacific.

Efficiency of the WES feedback

Following previous studies[21,40,43], the efficiency of the WES feedback (, representing change in the surface latent heat flux per unit anomalies of the surface wind) is expressed as follows:

$$\alpha = \frac{\partial LH}{\partial u} \approx \frac{u}{\sqrt{u^2 + w'^2}} = \frac{1}{\sqrt{1 + \left(\frac{w'}{u}\right)^2}}$$

Here w represents the background wind speed perturbation, is the background mean zonal wind. It should be mentioned that the zonal wind component dominants the change in the WES feedback, and

thus the contribution of the meridional wind is not considered[21,40,43].

AL and NPO

We use EOF analysis to obtain the AL and NPO variation patterns. The first two leading EOF modes of March SLP anomalies over North Pacific (20^o-70^{o}N, 120^{o}E-100^{o}W) during 1979-2019 are shown in Supplementary Figure 1. EOF1 is characterized by same-sign SLP anomalies over mid-high latitudes of the North Pacific, with the largest loading around the region where the climatological Aleutian Low generally is located. Thus, EOF1 represents variation of the Aleutian Low intensity (ALI). According to the spatial pattern shown in Supplementary Fig. 1a, we define an ALI as region-mean SLP anomalies over the area of 30^o-65^{o}N, 160^{o}E-140^{o}W. Note that positive value of ALI corresponds to a weakened AL intensity. The correlation coefficient between the ALI and the principal component (PC) time series of EOF1 is as high as 0.95 over 1979-2019. EOF2 of the SLP anomalies over the North Pacific is featured by a meridional dipole pattern, which represents the NPO (Supplementary Fig. 1b). The NPO index is defined as the PC time series corresponding to the EOF2 of SLP anomalies.

AMO

The Atlantic Multidecadal Oscillation (AMO) is the dominant SST variability on the multidecadal time scale in the North Atlantic[44]. Monthly mean smoothed AMO index since the January 1948 is obtained from the NOAA Physical Science Division (Fig. 5a). A positive (negative) AMO phase is defined as those years when the normalized AMO index is larger (smaller) than zero.

PDO

The Pacific Decadal Oscillation (PDO) is the first leading mode of SST variability on the decadal time scale over the North Pacific[57]. Monthly mean PDO index is extracted from the NOAA Physical Sciences Laboratory available from January 1948 to the present (Supplementary Fig. 6a). A positive (negative) PDO phase is defined as those years when the normalized PDO index is larger (smaller) than zero.

NPGO

The North Pacific Gyre Oscillation (NPGO) is the second EOF mode of sea surface height variation over the North Pacific, and it is characterized by interdecadal changes in the oceanic gyres over the subtropical and subpolar North Pacific[58]. Monthly mean North Pacific Gyre Oscillation (NPGO) index is derived from http://www.o3d.org/npgo/, covering the period from January 1950 to the present (Fig. 5b). A

positive (negative) NPGO phase is defined as those years when the normalized NPGO index is larger (smaller) than zero.

ENSO variability

ENSO variability is characterized by the Niño-3.4 SST index, which is defined as region-mean SST anomalies over 5^oS-5^oN, 120^o-170^oW. As ENSO has a strong quasi-biennial oscillation feature and has a strong impact on the AL, we remove preceding winter (December-March-mean, DJFM) Niño-3.4 SST index influence from the March AL index and all other variables based on a linear regression. This ensures that the connection of the March AL with the following winter ENSO is independent of the influence of preceding ENSO.

Statistical significance

Long-term linear trend and climatological seasonal cycle of all variables have been removed. Significance levels of regression and correlation coefficients are estimated by a two-tailed Student's *t* test.

Fisher's r-z transformation

Fisher's r-z transformation is used to estimate significance level of the difference between two correlation coefficients (denoted as R_1 and R_2). The Fisher transform of R_1 and R_2 can be written as follows[59]:

$$Z_1 = \frac{1}{2}\ln\left[\frac{1+R_1}{1-R_1}\right],$$

$$Z_2 = \frac{1}{2}\ln\left[\frac{1+R_2}{1-R_2}\right].$$

Then, the standard parametric test is employed to estimate the null hypothesis of the equality of the Z_1 and Z_2. The test statistic u is written as:

$$u = (Z_1 - Z_2)/[1/(N_1 - 3) + 1/(N_2 - 3)]^{1/2},$$

Here, N_1 and N_2 are the sizes of the data used to calculate R_1 and R_2, respectively. The test statistic u is normal distribution. Hence, the significance levels are evaluated based on the two-tailed Student's *t* test.

References

47. Kalnay, E. et al. The NCEP/NCAR 40-year reanalysis project. Bull. Am. Meteorol. Soc. 77(3), 437–472 (1996).

48. Huang, B. et al. Extended Reconstructed Sea Surface Temperature version 5 (ERSSTv5), Upgrades, validations, and intercomparisons. J. Clim. 30, 8179–8205 (2017).

49. Xie, P. & Arkin, P.A. Global precipitation: A 17-year monthly analysis based on gauge observations, satellite estimates, and numerical model outputs. Bull. Amer. Meteor. Soc. 78, 2539– 2558 (1997).

50. Saha, S. et al. The NCEP Climate Forecast System. J. Clim. 19, 3483–3517 (2006).

51. Eyring, V. et al. Overview of the Coupled Model Intercomparison Project Phase 6 (CMIP6) experimental design and organization. Geosci. Model. Dev. 9,1937–1958 (2016).

52. Rondeau-Genesse, G. & Braun, M. Impact of internal variability on climate change for the upcoming decades: analysis of the CanESM2-LE and CESM-LE large ensembles. Clim. Chang. 156, 299–314 (2019).

53. Yu, B., Li, G., Chen, S.-F. & Lin, H. The role of internal variability in climate change projections of North American surface air temperature and temperature extremes in CanESM2 large ensemble simulations. Clim. Dynam. 55, 869–885 (2020).

54. Deser, C., Phillips, A. S., Bourdette, V. & Teng, H. Uncertainty in climate change projections: the role of internal variability. Clim. Dynam. 38,527–546 (2012).

55. Vuuren, D. P. et al. The representative concentration pathways: an overview. Clim. Chan. 109, 5–31 (2011).

56. Zheng, Y.-Q., Chen, W. & Chen, S.-F. Intermodel spread in the impact of the springtime Pacific Meridional Mode on following-winter ENSO tied to simulation of the ITCZ in CMIP5/CMIP6. Geophys. Res. Lett. 48, e2021GL093945 (2021).

57. Mantua, N. J., Hare, S. R., Zhang, Y., Wallace, J. M. & Francis, R. A Pacific interdecadal climate oscillation with impacts on salmon production. Bull. Amer. Meteor. Soc. 78, 1069–1079 (1997).

58. Di Lorenzo, E. et al. North Pacific Gyre Oscillation links ocean climate and ecosystem change. Geophys. Res. Lett. 35, L08607 (2008).

59. Fisher, R. A. On the ‘probable error’ of a coefficient of correlation deduced from a small sample. Metron. 1, 3–32 (1921).

References

1. Bjerknes, J. Atmospheric teleconnections from the equatorial Pacific. *Mon. Weather Rev*. **97**, 163–172 (1969).
2. Jin, F.-F. Tropical ocean–atmosphere interaction, the Pacific Cold Tongue, and the El Niño–Southern Oscillation. *Science* **274**, 76–78 (1996).
3. Neelin, J. D. et al. ENSO theory. *J. Geophys. Res*. **103**, 14261–14290 (1998).
4. McPhaden, M. J., Zebiak, S. E. & Glantz, M. H. ENSO as an integrating concept in Earth science. *Science* **314**, 1740–1745 (2006).
5. Wang, B., Wu, R. & Fu, X. Pacific–East Asian teleconnection: How does ENSO affect EastAsian climate? *J. Clim.* **13**, 1517–1536 (2000).
6. Alexander, M. A. et al. The atmospheric bridge: The influence of ENSO teleconnections on air-sea interaction over the global oceans. *J. Clim.* **15**, 2205–2231 (2002).
7. Xie, S.-P. et al. Indian ocean capacitor effect on Indo-Western Pacific climate during the summer following El Niño. *J. Clim*. **22**, 730–747 (2009).
8. Zhang, R.-H., Min, Q.-Y. & Su, J.-Z. Impact of El Niño on atmospheric circulations over East Asia and rainfall in China: role of the anomalous western North Pacific anticyclone. *Sci. China Ear. Sci*. **60**, 1124–1132 (2017).
9. Yeh, S.-W. et al. ENSO atmospheric teleconnections and their response to greenhouse gas forcing. *Reviews of Geophysics* **56**, 185–206 (2018).
10. Cai, W. et al. Climate impacts of the El Niño–Southern Oscillation on South America. *Nat. Rev. Earth Environ*. **1**, 215–231 (2020).
11. Barnston, A. G., Tippett, M. K., L'Heureux, M. L., Li, S. & DeWitt, D. G. Skill of real-time seasonal ENSO model predictions during 2002–11: Is our capability increasing? *Bull. Amer. Meteorol. Soc*. **93**, 631–651 (2012).
12. Xue, Y., Chen, M. Y., Kumar, A., Hu, Z. & Wang, W. Q. Prediction skill and bias of tropical Pacific sea surface temperatures in the NCEP Climate Forecast System Version 2. *J. Clim*. **26**, 5358–5378 (2013).
13. Ashok, K., Behera, S., Rao, A. S., Weng, H. & Yamagata, T. El Niño Modoki and its teleconnection. *J. Geophys. Res*. **112**, C11007 (2007).
14. Kao, H.-Y. & Yu, J.-Y. Contrasting eastern Pacific and central Pacific types of ENSO. *J. Clim.* **22**, 615–632 (2009).
15. Kug, J.-S., Jin, F.-F. & An, S.-I. Two types of El Niño events: Cold tongue El Niño and warm pool El Niño. *J. Clim.* **22**, 1499–1515 (2009).
16. Linkin, M. E. & Nigam, S. The north pacific oscillation-west Pacific teleconnection pattern: mature-phase structure and winter impacts. *J. Clim.* **21**, 1979–1997 (2008).

17. Anderson, B. T. Tropical Pacific sea-surface temperatures and preceding sea level pressure anomalies in the subtropical North Pacific. *J. Geophys. Res.* **108**, 4732 (2003).
18. Yu, J.-Y. & Kim, S. T. Relationships between extratropical sea level pressure variations and the central Pacific and eastern Pacific types of ENSO. *J. Clim.* **24**, 708–720 (2011).
19. Yu, J.-Y., Lu, M.-M. & Kim, S. T. A change in the relationship between tropical central Pacific SST variability and the extratropical atmosphere around 1990. *Environ. Res. Lett.* **7**, 034025 (2012).
20. Yeh, S.-W., Wang, X., Wang, C. & Dewitte, B. On the relationship between the North Pacific climate variability and the central Pacific El Niño. *J. Clim.* **28**, 663–677 (2015).
21. Amaya, D. J. The Pacific Meridional Mode and ENSO: a Review. *Current Climate Change Reports*, **5**, 296–307 (2019).
22. Anderson, B. T. & Perez, R. C. ENSO and non-ENSO induced charging and discharging of the equatorial Pacific. *Clim. Dynam.* **45**, 2309–2327 (2015).
23. Chakravorty, S. R. C., Perez, B. T., Anderson, B. S., Giese, S. M. & Larsonand Pivotti, V. Testing the Trade Wind Charging mechanism and its influence on ENSO variability. *J. Clim.* **33**, 7391–7411 (2020).
24. Park, J.-H. et al. Role of the climatological intertropical convergence zone in the seasonal footprinting mechanism of the El Niño-Southern Oscillation. *J. Clim.* **34**, 5243–5256 (2021).
25. Wang, S. Y., L'Heureux, M. & Yoon, J. Are Greenhouse Gases Changing ENSO Precursors in the Western North Pacific? *J. Clim.* **26**, 6309-6322 (2013).
26. Horel, J. D. & Wallace, J. M. Planetary-scale atmospheric phenomena associated with the Southern Oscillation. *Mon. Weather Rev.* **109**, 813–829 (1981).
27. Straus, D. M. & Shukla, J. Distinguishing between the SST-forced variability and internal variability in mid latitudes: Analysis of observations and GCM simulations. *Quart. J. Roy. Meteor. Soc.* **126**, 2323–2350 (2000).
28. Chen, S.-F., Chen, W., Wu, R., Yu, B. & Graf, H. F. Potential impact of preceding Aleutian Low variation on the El Niño-Southern Oscillation during the following winter. *J. Clim.* **33**, 3061–3077 (2020).
29. Chang, P. et al. Pacific meridional mode and El Niño-Southern Oscillation. *Geophys. Res. Lett.* **34**, L16608 (2007).
30. Chiang, J. C. H., & Vimont, D. J. Analogous Pacific and Atlantic meridional modes of tropical atmosphere-ocean variability. *J. Clim.* **17**, 4143–4158 (2004).
31. Xie, S.-P. & Philander, S. G. H. A coupled ocean-atmosphere model of relevance to the ITCZ in the eastern Pacific. *Tellus* **46A**, 340–350 (1994).
32. Vimont, D. J., Wallace, J. M. & Battisti, D. S. The seasonal footprinting mechanism in the Pacific: Implications for ENSO. *J. Clim.* **16**, 2668–2675 (2003).
33. McPhaden, M. J. Tropical Pacific Ocean heat content variations and ENSO persistence barriers. *Geophys. Res. Lett.* **30**,1480 (2003).

34. Meinen, C.S., & McPhaden, M. J. Observations of warm water volume changes in the equatorial Pacific and their relationship to El Niño and La Niña. *J. Clim.* **13**, 3551–3559 (2000).
35. Lau, N.-C. Variability of the observed midlatitude storm tracks in relation to low-frequency changes in the circulation pattern. *J. Atmos. Sci*. **45**, 2718–2743 (1988).
36. Cai, M., Yang, S., van den Dool, H. & Kousky, V. Dynamical implications of the orientation of atmospheric eddies: A local energetics perspective. *Tellus* **59A**, 127–140 (2007).
37. Jin, F.-F. Eddy-induced instability for low-frequency variability. *J. Atmos. Sci*. **67**, 1947–1964 (2010).
38. Jin, F.-F., Pan, L. & Watanabe, M. Dynamics of synoptic eddy and low-frequency flow interaction. Part I: a linear closure. *J. Atmos. Sci*. **63**, 1677–1694 (2006).
39. Chen, S.-F, Yu, B. & Chen, W. An interdecadal change in the influence of the spring Arctic Oscillation on the subsequent ENSO around the early 1970s. *Clim. Dynam.* **44**, 1109–1126 (2015).
40. Vimont, D. J., Alexander, M. & Fontaine, A. Midlatitude excitation of tropical variability in the Pacific: The role of thermodynamic coupling and seasonality. *J. Clim.* **22**, 518–534 (2009).
41. Lin, C. Y., Yu, J.-Y. & Hsu, H.-H. CMIP5 model simulations of the Pacific meridional mode and its connection to the two types of ENSO. *Int. J. Climatol*. **35**, 2352–2358 (2014).
42. Yu, J.-Y. et al. Linking emergence of the central-Pacific El Niño to the Atlantic Multi-decadal Oscillation. *J. Clim*. **28**, 651–662 (2015).
43. Vimont, D. J. Transient growth of thermodynamically coupled variations in the tropics under an equatorially symmetric mean state. *J. Clim.* **23**, 5771–89 (2010).
44. Kerr, R. A. A North Atlantic climate pacemaker for the centuries. *Science* **288**, 1984–1985 (2000).
45. Wang, L., Yu, J.-Y. & Paek, H. Enhanced biennial variability in the Pacific due to Atlantic capacitor effect. *Nat. Commun.* **8**, 14887 (2017).
46. Yu, J.-Y. Enhancement of ENSO's persistence barrier by biennial variability in a coupled atmosphere-ocean general circulation model. *Geophys. Res. Lett*. **32**, L13707 (2005).

Figures

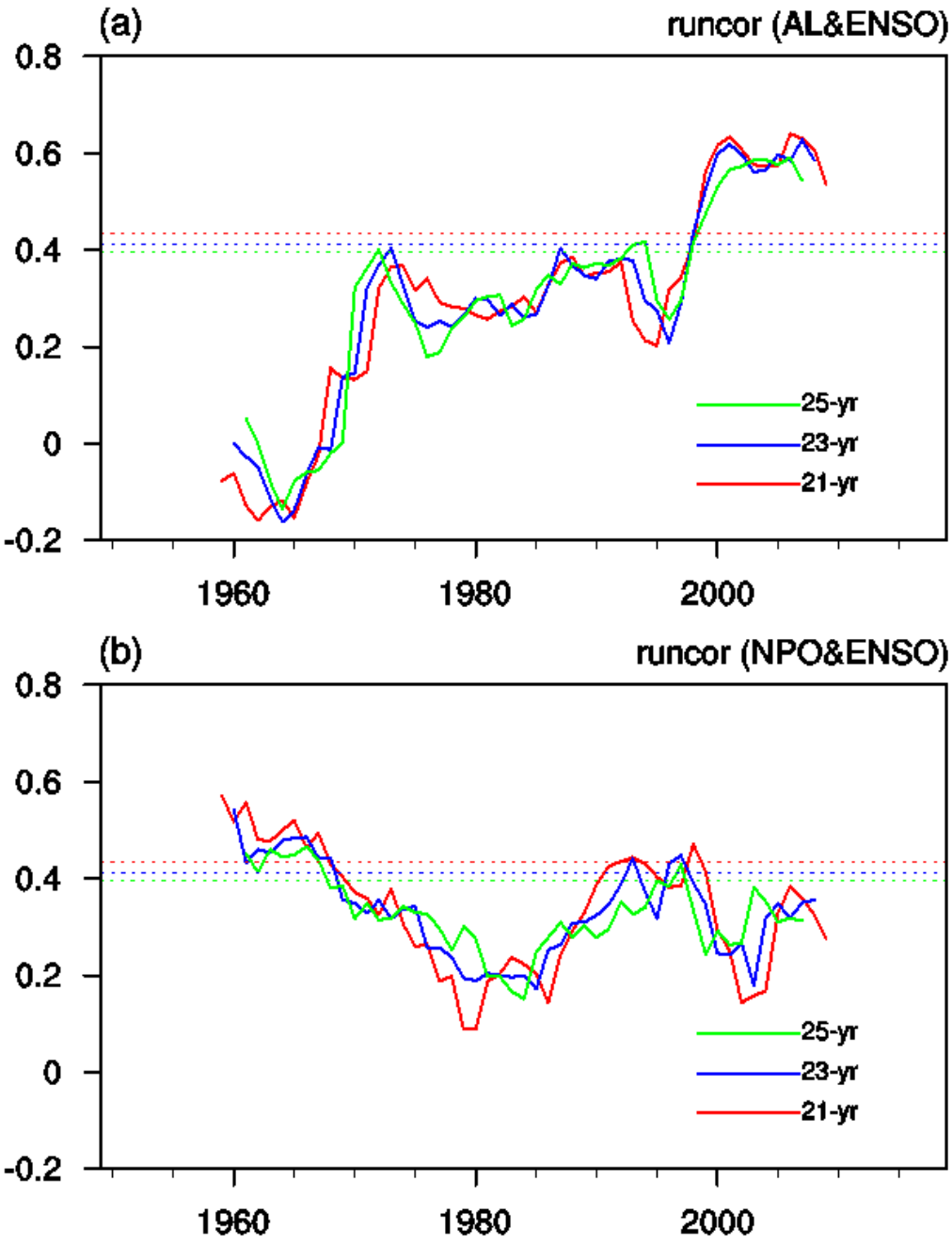

Figure 1

Correlations of ENSO with preceding AL and NPO. Running correlation coefficients of **(a)** the early-spring (March) ALI and **(b)** the winter (December-January-February-mean, DJF) NPO index with the following winter (D(0)JF(1)) Niño-3.4 SST index with different moving lengths. Horizontal lines indicate the corresponding running correlations significant at the 95% confidence level. Years in (a) and (b) denote the central years of the moving correlation.

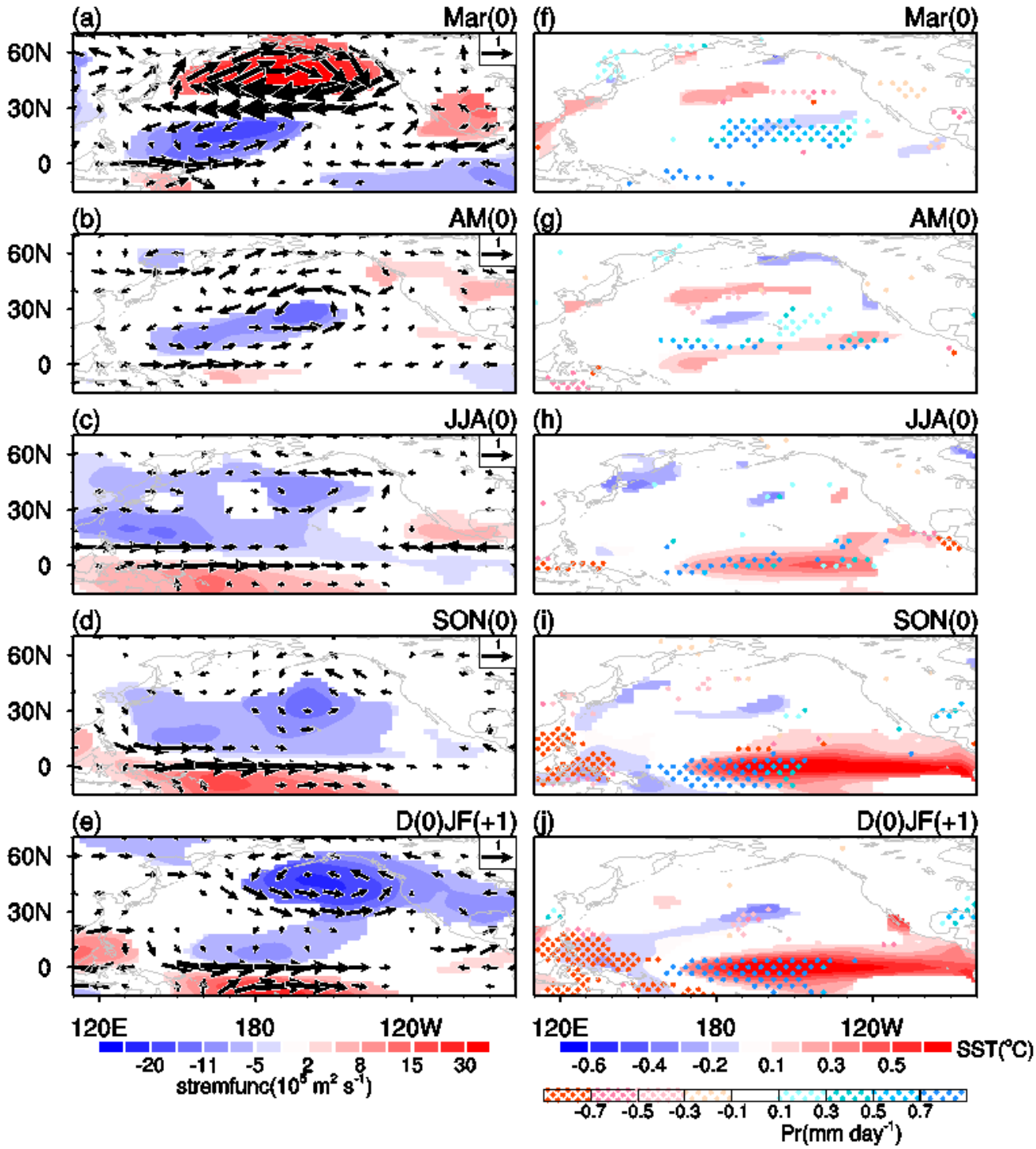

Figure 2

Evolutions of SST and atmospheric anomalies related to the spring AL. Anomalies of 850-hPa stream function (shading) and winds (vector) in **(a)** March(0), **(b)** AM(0), **(c)** JJA(0), **(d)** SON(0), and **(e)** D(0)JF(1) regressed upon the normalized ALI in March(0) over 1996-2018. **(f-j)** as in **(a-e)**, but for the evolutions of SST (shading) and precipitation (stippling) anomalies. Only the SST, precipitation and stream function anomalies exceeding the 95% confidence level are shown.

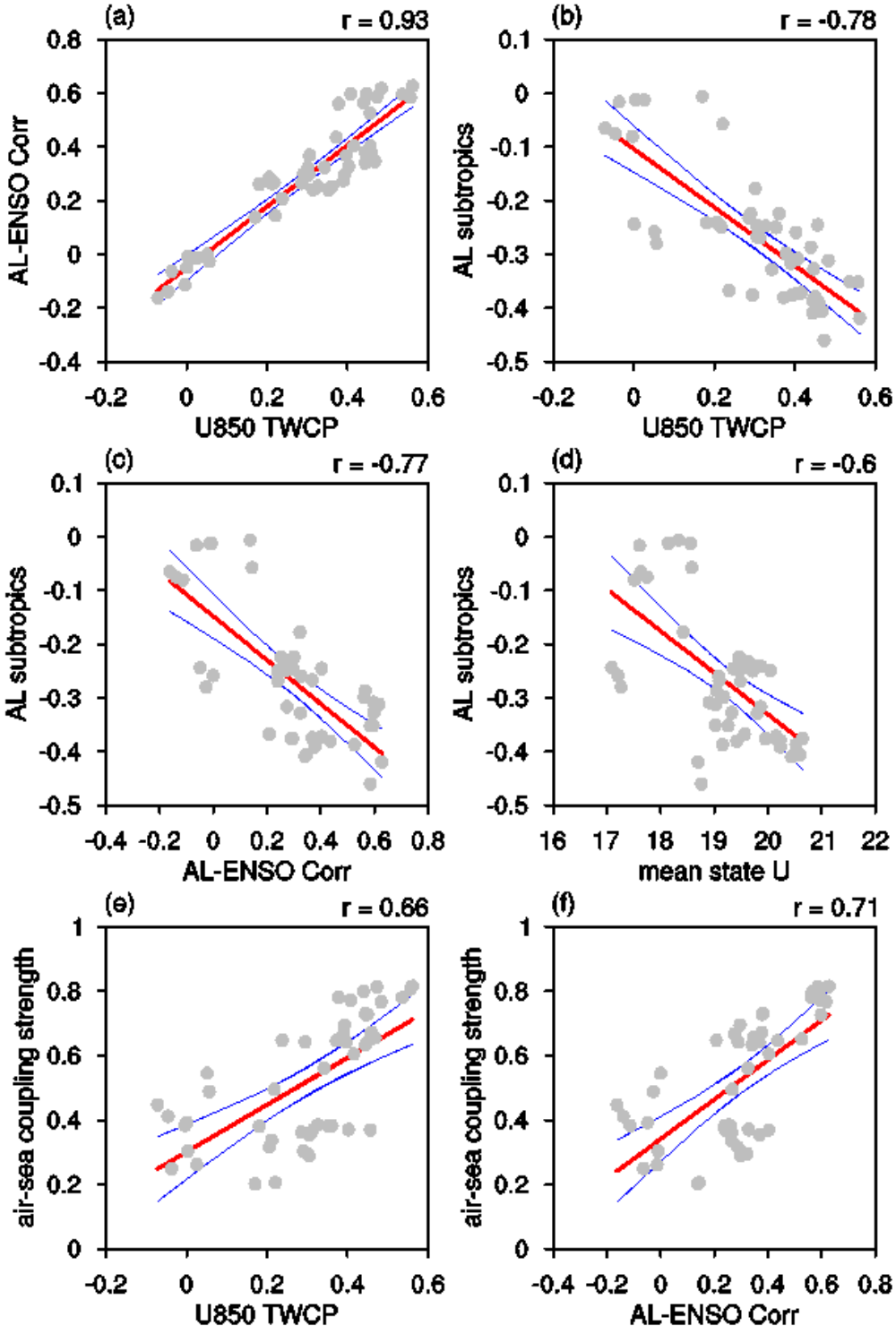

Figure 3

Factors contributing to change in the AL-ENSO connection. Scatter plots of the spring ALI-related 850-hPa winds anomalies averaged over tropical western-central Pacific (region in Supplementary Fig. 3b) for 23-yr running period against **(a)** the 23-yr running correlations between the spring ALI and winter Niño3.4 SST index, and against **(b)** the spring SLP anomalies averaged over subtropical North Pacific (region in Supplementary Fig. 3a). Scatter plots of the spring SLP anomalies averaged over subtropical North Pacific against **(c)** the 23-yr running correlations of spring AL and winter Niño3.4 SST index, and against

(d) the climatology of 500-hPa zonal wind averaged over mid-latitude North Pacific (27.5°N-32.5°N,135°E-130°W). Scatter plots of the air-sea coupling strength over the subtropical northeastern Pacific (Methods) against **(e)** the 850-hPa zonal wind anomalies averaged over the tropical western-central Pacific, and against **(f)** the 23-yr running correlations between the spring ALI and winter Niño3.4 SST index. Red lines indicates the best linear fit. Blue lines indicate the 95% confidence range of the linear regression.

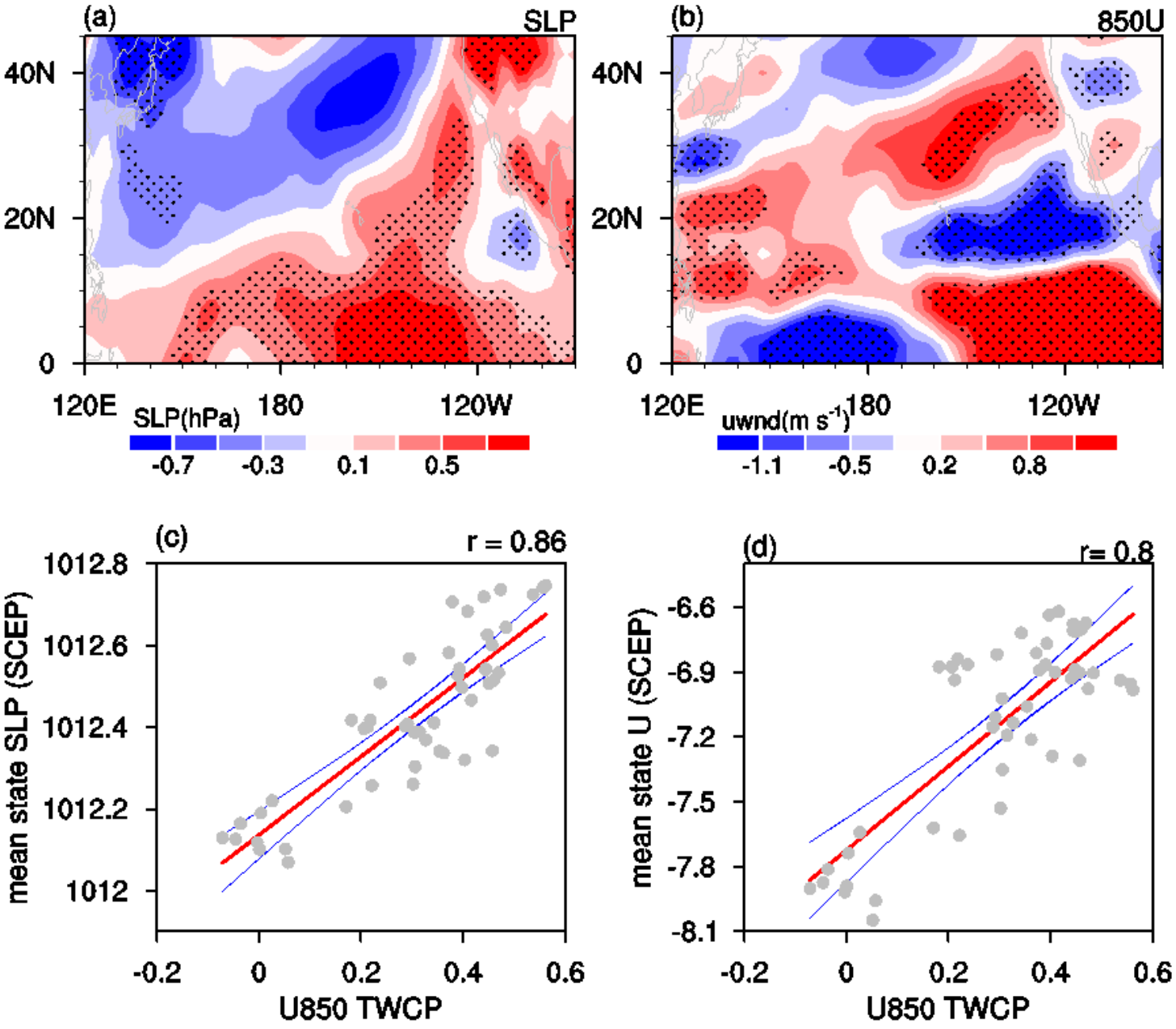

Figure 4

Differences in the mean states. Differences in the climatology of spring **(a)** SLP (hPa) and **(b)** 850-hPa zonal wind (m s^{-1}) between periods 1996-2018 and 1949-1995. Stippling regions in **(a-b)** indicate the differences that are significantly different from zero at the 95% confidence level. Scatter plots of the spring ALI-related 850-hPa zonal wind anomalies averaged over the tropical western-central Pacific against the climatology of spring **(c)** SLP and **(d)** 850-hPa zonal wind over the subtropical northeastern Pacific for the 23-yr running period. Red lines indicate the best linear fit. Blue lines indicate the 95% confidence range of the linear regression.

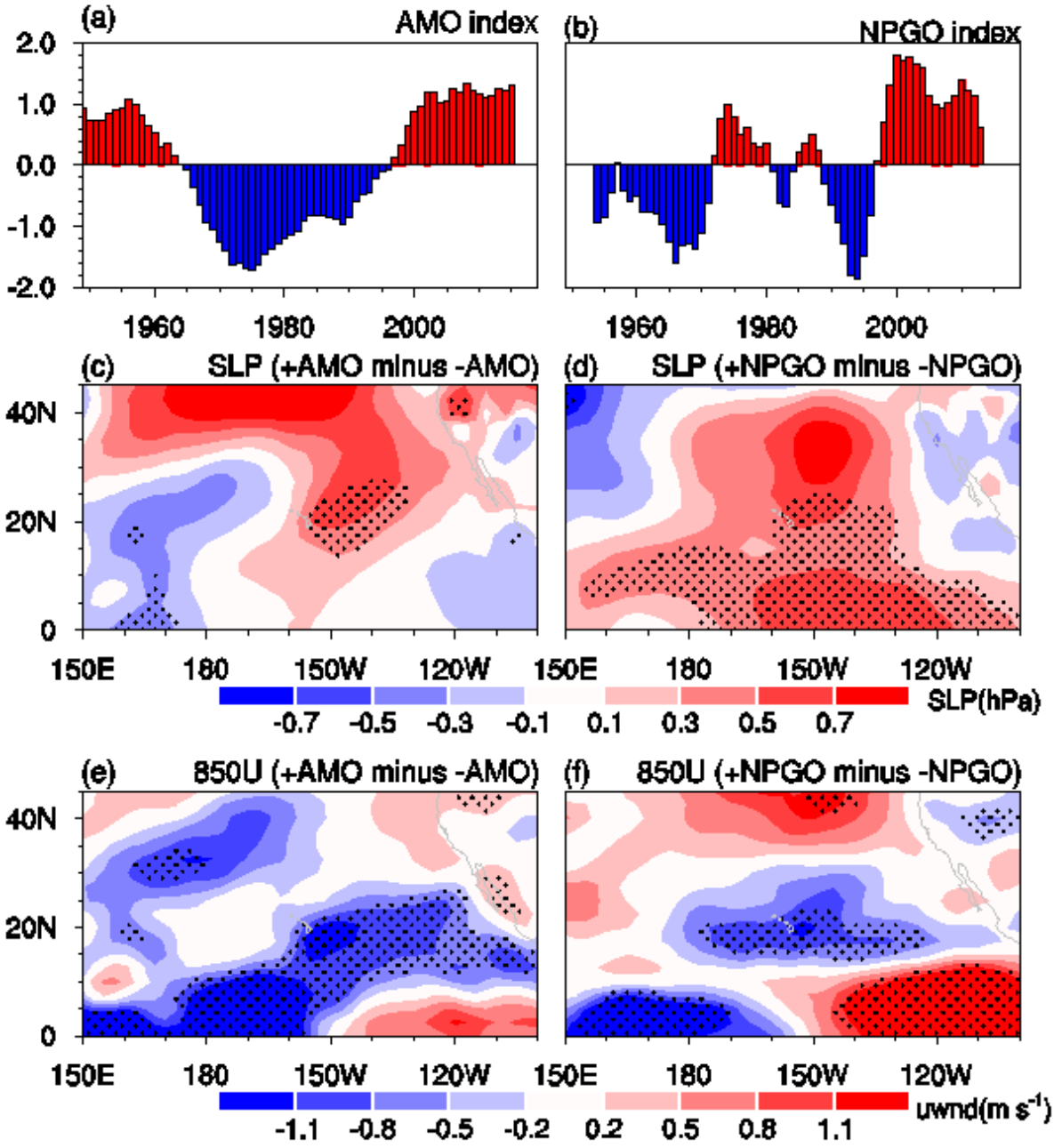

Figure 5

Modulations of the AMO and NPGO. Normalized time series of the spring (a) smoothed AMO index and (b) NPGO index with 9-year running mean. Differences in the climatology of spring SLP (hPa) (c) between positive and negative AMO phases, and (d) between positive and negative NPGO phases. (e-f) as in (c-d), but for differences in the climatology of spring 850-hPa zonal wind (m s^{-1}) between different phases of the AMO and NPGO. Stippling regions in (c-f) indicate the differences that are significantly different from zero at the 95% confidence level.

Supplementary Files

This is a list of supplementary files associated with this preprint. Click to download.

- Supplementaryinformation.doc